PNAS RESEARCH ARTICLE | MICROBIOLOGY

Mutualism between degraders and nondegraders stabilizes the function of a natural biopolymer-degrading community

Liang Liu[a], Changfu Tian[b], Miaoxiao Wang[c,d], Ying Luo[a], Yaru Huang[a], Tingting Jiang[a], Hongwen Zhao[a], Qijun Yu[a], Entao Wang[e], Jinshui Yang[a,1], and Hongli Yuan[a,1]

Affiliations are included on p. 12.

Edited by James McKinlay, Indiana University, Bloomington, IN; received January 16, 2025; accepted June 18, 2025 by Editorial Board Member Caroline S. Harwood

Natural biopolymer-degrading microbial communities drive carbon biogeochemical cycling. Within these communities, polymer degraders facilitate the growth of nondegraders by breaking down polymers through extracellular enzymes. However, the contributions of nondegraders to community dynamics, as well as the mechanisms that limit their access to degradation products, remain poorly understood. Here, we investigate EMSD5, a lignocellulose-degrading microbial community that efficiently converts corncob into isopropanol. We demonstrate that nondegraders, such as *Escherichia coli*, enable the growth of degraders (e.g., *Lachnoclostridium* sp. and *Clostridium beijerinckii*) by creating anaerobic conditions and supplying biotin. Within such expanded niches, lignocellulose degradation proceeds sequentially, and the availability of breakdown products to *E. coli* is constrained by two interlinked processes. Specifically, *Lachnoclostridium* sp. produces oligosaccharides that are largely inaccessible to *E. coli*. A subset of these oligosaccharides is utilized by *C. beijerinckii* to produce monosaccharides that support *E. coli* growth, while glycosidase secretion by *C. beijerinckii* is reduced under coculture conditions. Building on these findings, we designed a synthetic consortium by coculturing *C. beijerinckii* with an engineered *E. coli* strain that expresses xylanase genes from an unculturable *Lachnoclostridium*. This consortium achieved isopropanol production from hemicellulose without requiring anaerobic conditions. Our findings reveal the niche-expanding role of nondegraders and the processes that constrain their access to degradation products, offering insights into maintaining stable cooperation in biopolymer-degrading communities and designing efficient consortia for biopolymer conversion.

mutualistic interaction | nondegrader | niche expansion | exploitation alleviation | biopolymer degradation

Significance

Biopolymer degradation is essential for carbon cycling, yet the roles of nondegrading microbes and the mechanisms by which degraders limit resource exploitation remain unclear. Our study reveals roles for nondegraders in expanding the niches of degraders by establishing early anoxic conditions and supplying biotin. Within such niches, resource partitioning arising from substrate-specific enzymes and reduced enzyme secretion in degraders limit the availability of breakdown products to nondegraders. Leveraging these insights, we engineered synthetic consortia that convert hemicellulose into isopropanol without requiring anaerobic pretreatment. These findings provide evidence of microbial mutualism in expanding niches within natural ecosystems, advancing our understanding of how stable cooperation is maintained in natural biopolymer-degrading communities.

The biodegradation of biopolymers by heterotrophic microbial communities is important for biogeochemical cycling (1–3). Within these communities, the biochemical capacity for biopolymer degradation is typically distributed across diverse strains (4, 5). This functional distribution results in intricate interdependences, where the metabolic activities of one strain rely on those of others, promoting synergisms that enhance community resilience and efficiency. Therefore, maintaining stable interactions among diverse species is essential for biopolymer degradation (2, 6, 7).

Biopolymer degradation typically begins with specialized degraders that secrete extracellular enzymes to cleave biopolymers into transportable breakdown products (7, 8). The resulting polymer fragments serve as "public goods", accessible to both degraders and "nondegraders"—strains that cannot produce biopolymer-degrading enzymes (8–10). This dynamic creates a "tragedy of the commons" scenario, wherein nondegraders excessively utilize public goods without contributing to the collective degradation effort. Such exploitation has been shown to destabilize community structure and impair ecosystem functionality (11–13). Despite these challenges, cooperative interactions remain prevalent within biopolymer-degrading communities and are fundamental to shaping microbial community structure and evolutionary trajectories (2, 6, 14). Understanding how these interactions are regulated and how communities mitigate exploitation is essential for elucidating natural community assembly and designing efficient degradation consortia.

Extensive research has employed synthetic microbial communities to explore how cooperative partners manage exploitative behaviors in exchanging communally valuable nutrients, such as amino acids and vitamins (13, 15–17). However, the cross-feeding dynamics within biopolymer-degrading communities present unique features that the findings in nutrient-based systems cannot fully explain. For instance, extracellular enzymes secreted

The authors declare no competing interest.

This article is a PNAS Direct Submission. J.B.M. is a guest editor invited by the Editorial Board.

[1]To whom correspondence may be addressed. Email: yangjsh1999@cau.edu.cn or hlyuan@cau.edu.cn.

This article contains supporting information online at https://www.pnas.org/lookup/suppl/doi:10.1073/pnas.2500664122/-/DCSupplemental.

Published July 21, 2025.

by degraders are not directly consumable by other microbes and persist in the environment, continuously releasing breakdown products over extended periods. This persistence exacerbates the exploitation of degraders by nondegraders (11, 13). Although in soil or biofilm-dominated environments, diffusion may be significantly restricted due to physical barriers and matrix effects (13), in environments with high diffusion rates, such as the aquatic systems, approximately 99% of the breakdown products generated by extracellular enzymes diffuse away from the degraders before uptake (9). These dynamics suggest that degraders in biopolymer-degrading consortia must employ stringent regulatory mechanisms to control enzyme secretion and prevent overexploitation by nondegraders. Yet, the specific regulatory mechanisms underlying this control remain poorly understood. Furthermore, while degraders shape the assembly of nondegraders, nondegraders also affect the growth and behavior of degraders by cross-feeding (18, 19). However, little is known about whether nondegraders employ other mechanisms to influence the niches of degraders and how these interactions impact the overall efficiency and stability of biopolymer degradation within consortia.

To address these challenges, we focused on the context of the degradation of lignocellulose, the most abundant biopolymer on Earth (20). We enriched a lignocellulose-degrading community, EMSD5, from compost using corn stover as the sole carbon source (21). This community underwent over a hundred passages using the corn stover as the sole carbon source. Remarkably, the anaerobic members of EMSD5 coexisted stably and efficiently convert untreated lignocellulose, particularly hemicellulose, into isopropanol without requiring anaerobic treatment (22). Such stable composition and functional performance make EMSD5 suitable for exploring interactions between degraders and nondegraders in biopolymer degradation.

In this study, we reveal critical mutualistic interactions that underpin the stability and function of EMSD5. The aerobic nondegraders, such as *Escherichia coli*, act as pioneering populations that create anaerobic niches and increase the production of biotin, thus enabling the growth of anaerobic degraders like *Lachnoclostridium* sp. and *Clostridium beijerinckii*. Within such expanding niches, distinct mechanisms occurring in different degraders—resource partitioning and reduced enzyme secretion—constrain exploitation within the community. We used these insights to construct a synthetic consortium of *E. coli* and *C. beijerinckii* that efficiently converts hemicellulose into isopropanol. Our findings highlight the ecological role of the mutualism between degraders and nondegraders, providing a clue for developing synthetic consortia aimed at biopolymer conversion.

Results

Aerobic Nondegraders Thrive in the Initial Phase of Lignocellulose Bioconversion. To investigate the dynamic of EMSD5 and the potential roles of its members, the microbial community composition throughout the isopropanol production process was characterized. EMSD5 typically completes this process within 6 d, which was divided into three distinct phases based on the isopropanol productivity: the initial phase (day 1), the fast phase (day 2), and the stagnation phase (days 4 to 6) (Fig. 1*A*). High-throughput 16S rRNA gene sequencing revealed that EMSD5 is primarily composed of *Escherichia*, *Bacteroides*, *Clostridium*, *Lachnoclostridium*, and *Lysinibacillus*, collectively accounting for over 85% of the relative abundance across all samples (*SI Appendix*, Fig. S1*A*).

During the initial phase, aerobes, such as *Escherichia*, *Lysinibacillus*, and *Enterococcus*, dominated the community, with *Escherichia* alone achieving a relative abundance of 39.2%. However, its abundance decreased to 9.6% by day 4 and recovered to 21.3% by day 6. By contrast, the relative abundance of anaerobes, including *Lachnoclostridium*, *Clostridium*, and *Bacteroides*, increased from 49.9% on day 1 to 81.4% and 66.5% on days 4 and 6, respectively (Fig. 1*B* and *SI Appendix*, Fig. S1*A*). Linear Discriminant Analysis Effect Size identified *Escherichia* as the distinguishing operational taxonomic unit (OTU) in the initial phase, while *Lachnoclostridium* and *Clostridiales* were enriched in the fast phase (Fig. 1*C*). By the stagnated phase, the relative abundance of *Clostridium* remained stable, with *Bacteroides* emerging as the distinguishing OTU (*SI Appendix*, Fig. S1*B*). The similarity in community compositions between the fourth and 6 days (*SI Appendix*, Fig. S1*C*), with no distinct discriminating species, indicates a stabilization of the community composition by the stagnation phase. Thus, EMSD5 transitions from an aerobe-dominated community to an anaerobe-dominated community as the process progresses.

To investigate the interactions between different members, a sample collected on the 6 day was subjected to metagenomic sequencing (*SI Appendix*, Table S1). The binning process of contigs yielded 12 metagenome-assembled genomes (MAGs), of which 10 met quality thresholds [completeness >50%, contamination <15% (23)] and were classified into six genera: *Clostridium* (EM01, EM07, EM08, EM09, and EM10), *Lachnoclostridium* (EM03), *Lysinibacillus* (EM02), *Enterococcus* (EM04), *Bacteroides* (EM05), and *Escherichia* (EM11) (*SI Appendix*, Fig. S2 and Table S2). Analysis of glycoside hydrolase (GH) genes revealed that families responsible for cellulose and hemicellulose degradation were predominantly encoded by anaerobes, particularly *Lachnoclostridium* and *Clostridium* (Fig. 1*D* and Dataset S1). Pathway analysis indicated that only *C. beijerinckii* EM01 possesses a known complete isopropanol production pathway (*SI Appendix*, Fig. S3*A* and Datasets S2 and S3). These results demonstrate that while aerobes thrive in the initial phase, they function as nondegraders.

Aerobic Nondegraders Expand the Niche Space of *Clostridium* by Providing Anoxic Conditions and Biotin. Given the obligate anaerobic nature of *Clostridium* and the fact that the medium was not subjected to anaerobic treatment, we hypothesized that certain members of EMSD5 facilitate *Clostridium* growth by creating anaerobic niches. Analysis of oxidative phosphorylation pathways revealed that aerobes, including *E.* coli EM11, *Lysinibacillus* sp. EM02, and *Enterococcus* sp. EM04, possess *cydA* and *cydB*, genes essential for oxygen depletion (Fig. 1*D*, Datasets S2 and S3).

To test this hypothesis, we isolated *E. coli* (*Eco*), *Lysinibacillus* sp. (*Lys*), and *Enterococcus* sp. (*Ent*) under aerobic conditions, as well as *C. butyricum* (*Cbu*), *C. beijerinckii* (*Cbe*), and *C. magnum* (*Cma*) under anaerobic conditions. Consistent with bioinformatic analysis, *Cbe* was confirmed to ferment xylose or glucose to isopropanol (*SI Appendix*, Fig. S3*B*). We then inoculated nutrient-rich LB medium supplemented with 2 g/L xylose and 10 mg/L resazurin (a redox indicator that turns colorless upon oxygen depletion) with equal ratios of each aerobe and *Clostridium*, using *Cbe* as a representative strain. Both *Eco* monoculture and *Eco-Cbe* coculture decolorized resazurin within 2 h, indicating rapid oxygen consumption. In contrast, *Lys* and *Ent* took 24 h for complete color change (Fig. 2*A*). Parallel measurements of redox potential supported these observations: *Eco-Cbe* coculture reached a dramatic drop in redox potential to less than -300 mV within 2 h, whereas *Lys-Cbe* and *Ent-Cbe* cocultures only achieved modest reductions (–46 mV and –133 mV, respectively) after 12 h (Fig. 2*A*). These results were mirrored in aerobe monocultures (*SI Appendix*, Fig. S4). Accordingly, *Cbe* failed to grow alone but

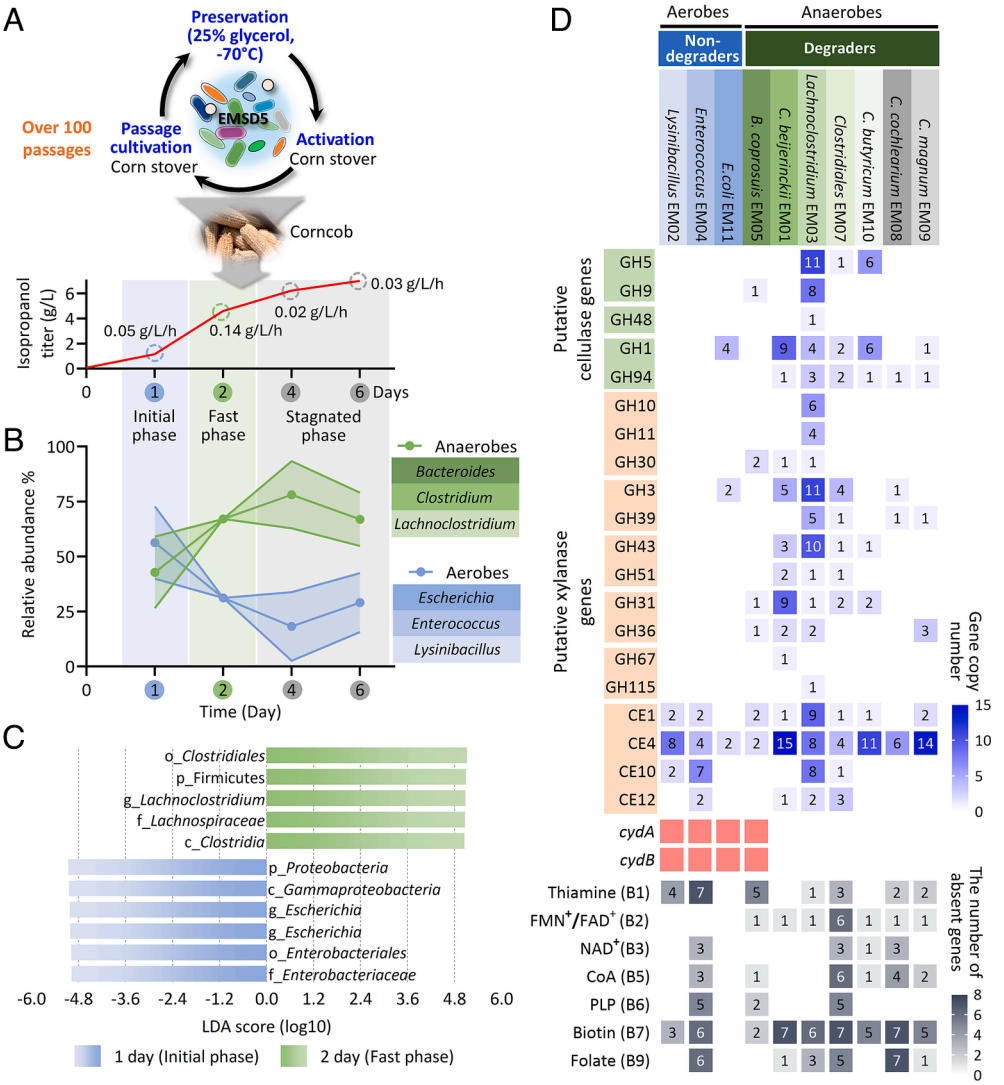

Fig. 1. Aerobic nondegraders dominate the initial phase of lignocellulose bioconversion. (*A*) Schematic of the lignocellulose-converting community EMSD5. This community has been passaged stably for more than 100 times using corn stover as the sole carbon source. EMSD5 exhibits the capability to convert untreated corncob to isopropanol. We previously categorized isopropanol production into three phases, including the initial phase (1 day), the fast phase (2 day), and the stagnated phase (4 and 6 day). (*B*) Relative abundances of anaerobes (*Clostridium*, *Lachnoclostridium*, and *Bacteroides*) and aerobes (*Escherichia*, *Lysinibacillus*, and *Enterococcus*) across the three phases, as determined using 16S rRNA gene amplicon sequencing. (*C*) Identification of bacterial genera that differentiate between the initial and rapid phases using linear discriminant analysis effect size (Kruskal–Wallis test) (LDA > 4.0, $P < 0.05$). The histogram illustrates the differentially abundant genera between the initial and rapid phases. (*D*) A heat map displaying the presence of genes and metabolic pathways in each metagenome-assembled genome (*Top*). Genes not detected in specific MAGs are represented by white. For hydrolase genes, the copy number across different MAGs is indicated with color scaling. For vitamin biosynthetic pathways, the number of absent genes within each pathway is documented with color scaling.

thrived in coculture with *Eco* without anaerobic treatment (Fig. 2*A*). Additionally, *Eco* grown alone in chemically defined media with unwashed corncob as a carbon source (rather than washed corncob), showed a decrease in glucose and xylose concentrations (*SI Appendix*, Fig. S5 *A* and *B*), indicating *Eco*'s ability to utilize soluble carbon for early growth and create an anaerobic environment for *Clostridium*.

Further analysis of vitamin synthesis pathways showed that *Lachnoclostridium* and *Clostridium* strains lacked complete pathways for specific vitamins, including biotin (VB7), FMN+/FAD+ (VB2), and folate (VB9). Notably, *E. coli* EM11 harbored complete pathways for multiple vitamins (Fig. 1*D* and Dataset S4), suggesting that *E. coli* may act as a primary vitamin provider. To investigate this, we examined the growth of *Cbe* in chemically defined media lacking VB7, VB2, or VB9. The absence of VB2 or VB9 had minimal effect, but the lack of VB7 severely impaired *Cbe* growth. Moreover, *Cbe* growth exhibited a concentration-dependent response to VB7 (*SI Appendix*, Fig. S6 *A* and *B*). Similarly, *Cbu* and *Cma* growth was also hindered in biotin-deficient chemically defined media (*SI Appendix*, Fig. S6*C*), indicating that biotin is a limiting nutrient for *Clostridium*. In contrast, *Eco* thrived without biotin or all tested vitamins (*SI Appendix*, Fig. S6*D*).

To determine whether *Eco* could support *Clostridium* growth via biotin provision, we inoculated a biotin-deficient chemically defined media with an equal ratio of *Eco* to *Clostridium* strains without anaerobic treatment. Compared to the monoculture of *Clostridium* in biotin-deficient chemically defined media, coculture with *Eco* led to 100-fold increases in *Clostridium* CFUs after 48 h ($P < 0.01$) (Fig. 2*B*). Interestingly, the coculture starting under anaerobic conditions resulted in decreased *Eco* growth, accompanied by a decline in *Cbe* CFUs at 144 and 192 h (*SI Appendix*, Fig. S7*A*). Pearson correlation analysis revealed a positive correlation between *Cbe* and *Eco* CFUs (*SI Appendix*, Fig. S7*B*), supporting a dependency of *Cbe* growth on *Eco*-derived biotin. To further validate this, we examined *Cbe* growth in sterile supernatants from a 48-h culture of *Eco* in biotin-deficient

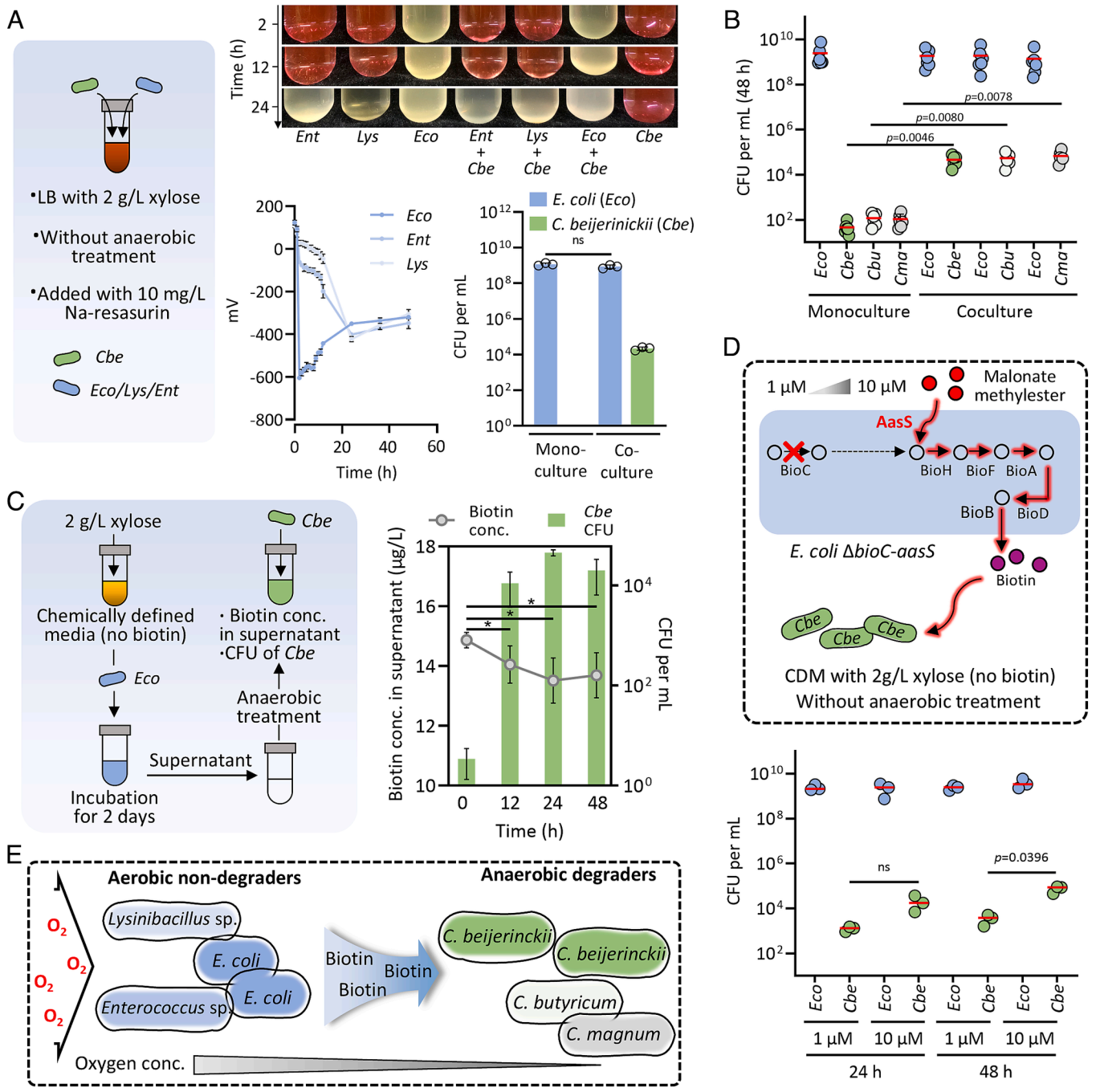

Fig. 2. Contribution of aerobic nondegraders to anaerobic conditions and biotin availability for *Clostridium*. (*A*) Oxygen depletion and growth dynamics in coculture systems. (*Top*) Time-course documentation of resazurin reduction (pink to colorless transition indicating oxygen depletion) in xylose-supplemented LB medium containing 10 mg/L resazurin, showing differential oxygen consumption rates among: *Eco*, *Lys*, and *Ent* monocultures; and their respective cocultures with *Cbe*. (*Bottom*) The redox potentials of various coculture systems were recorded, alongside the enumeration of colony-forming units (CFUs) of *Cbe* in both monoculture and coculture with *Eco* (n = 3). Date is represented as mean ± SEM. *P* value derived from unpaired two-tailed Student's *t* test, "ns" for nonsignificant comparison. (*B*) Comparison of CFUs for *Clostridium* strains in monoculture versus coculture with *Eco* (n = 6). *P* values derived from Welch's *t* test. (*C*) CFU counts for *Cbe* cultured using sterile-filtered supernatant collected from a 48-h culture of *Eco*, with biotin concentration in the supernatant also measured using a biotin quantitative kit (n = 3). *P* values derived from one-way ANOVA with the Tukey test; statistical significance indicated as $*P < 0.05$. (*D*) Comparison of CFUs for *Cbe* in coculture with *Escherichia coli* Δ*bioC*-aasS at varying concentrations of malonate methylester (1 µM and 10 µM) (n = 3). *P* values derived from Welch's *t* test, "ns" for nonsignificant comparison. (*E*) Schematic for aerobic nondegraders construct suitable niches to facilitate the growth of anaerobic degraders.

chemically defined media. As expected, the biotin concentration in the supernatant decreased ($P < 0.05$) as *Cbe* grew (Fig. 2*C*).

We then generated a Δ*bioC* mutant of *Eco*. This mutant failed to grow in biotin-deficient chemically defined media (*SI Appendix*, Fig. S8*A*) but outperformed the wild type in the LB medium (*SI Appendix*, Fig. S8*B*), indicating a growth cost associated with biotin synthesis. To bypass the *bioC* requirement, we introduced an acyl-ACP synthetase (AasS) from *Vibrio harveyi* (24), enabling the mutant to synthesize biotin from malonate methylester, a compound unusable by *Cbe* (*SI Appendix*, Fig. S9). Cocultures of *Cbe* with *Eco* ΔbioC-aasS in biotin-deficient chemically defined media supplemented with malonate methylester showed significantly improved *Cbe* growth at 10 µM malonate methylester compared to 1 µM ($P = 0.04$) (Fig. 2*D*), confirming *E. coli*'s role in biotin provision.

Together, these findings demonstrate that aerobic nondegraders, especially *Eco*, enable *Clostridium* colonization by rapidly

consuming oxygen and providing biotin (Fig. 2*E*), thereby fostering a symbiotic relationship.

***Lachnoclostridium* sp. EM03 and *C. beijerinckii* EM01 Release Breakdown Products From Hemicellulose By Mutualistic Interactions.** The release of breakdown products by degraders influences both the assembly and invasion of nondegraders (2, 8, 25). Therefore, we focused on this process within the EMSD5 by profiling extracellular GHs responsible for the degradation of untreated corncob and its different polysaccharide components, including hemicelluloses (beechwood xylan; wheat arabinoxylan) and cellulose (filter paper). Mass spectrometry, combined with GH annotation across MAGs, identified *Lachnoclostridium* sp. EM03 and *C. beijerinckii* EM01 as the main producers of extracellular GHs (Fig. 3*A* and *SI Appendix*, Fig. S10 and Dataset S5).

Given the heterogeneity and recalcitrance of hemicellulose (26), we focused on xylan breakdown. When induced by beechwood xylan, composed of xylose units with rare substitutions, EM03 secreted two GH11 enzymes (IDs: 1087 and 1090) and one GH30 enzyme (ID: 3096). Meanwhile, EM01 secreted two GH3 enzymes (IDs: 2177 and 3080) and one GH43 enzyme (ID: 2178) (Fig. 3*A* and *SI Appendix*, Fig. S10 and Dataset S5). Hydrolytic assays revealed that EM03's GH11 enzymes exhibited xylanase activity, producing xylo-oligosaccharides, while EM01's GH43 and GH3 enzymes acted as β-xylosidases, hydrolyzing xylo-oligosaccharides to release xylose (*SI Appendix*, Fig. S11 *A–C*). Based on the proteomics-derived abundance of these enzymes, we constructed two enzyme cocktails: a xylanase cocktail from EM03 (Xyn_1) containing GH11 and GH30 enzymes and a xylosidase cocktail from EM01 (Xylo_1) containing GH3 and GH43 enzymes. Xyn_1 effectively released reducing sugars from beechwood xylan but produced little xylose. Xylo_1 alone had no activity on beechwood xylan. However, combining Xyn_1 and Xylo_1 significantly increased the production of both reducing sugars and xylose (Fig. 3*B* and *SI Appendix*, Fig. S11*D*).

For wheat arabinoxylan, a more complex hemicellulose containing xylose residues substituted with arabinose, EM03 secreted additional GH10 xylanases (IDs: 1130 and 2041) and another GH11 xylanase (ID: 1088). EM01 secreted two additional GH51 enzymes (ID: 3534 and 3217) (Fig. 3*A* and *SI Appendix*, Fig. S10 and Dataset S5). Enzyme 3534 exhibited bifunctional glycosidase activity, releasing arabinose from mono- or disubstituted xylose residues and xylose from xylo-oligosaccharides. Enzyme 3217 targeted monosubstituted xylose residues (*SI Appendix*, Fig. S12 *A–C*). Accordingly, three enzyme cocktails were assembled: a xylanase cocktail from EM03 (Xyn_2), a xylosidase cocktail from EM01 (Xylo_2), and an arabinofuranosidase cocktail from EM01 (Abf). Xyn-2 alone hydrolyzed wheat arabinoxylan to reducing sugars but not xylose and arabinose release. Neither Xylo_2 nor Abf exhibited activity alone on arabinoxylan. However, combining Xyn_2 with Xylo_2 and Abf cocktail enhanced the release of xylose and arabinose, respectively. Adding both Xylo_2 and Abf to Xyn_2 resulted in the highest production of reducing sugars, particularly xylose and arabinose (Fig. 3*B* and *SI Appendix*, Fig. S12*D*).

These results reveal a mutualistic interaction in xylan degradation: EM03 breaks down complex hemicellulose into oligosaccharides, which are then further depolymerized by EM01 into monosaccharides (Fig. 3*C*).

Dual Limitations on Breakdown Product Availability Constrain Exploitation. While EM03 contributes substantially to lignocellulose degradation, the mechanisms underlying the restricted accessibility of its breakdown products remain unclear. To address this, we examined the consumption of breakdown products within the context of EMSD5, focusing on *Eco*, a highly abundant strain that plays essential roles in community function.

We first tested *Eco*'s ability to utilize beechwood xylan, wheat arabinoxylan, and their corresponding oligosaccharides produced by EM03-derived xylanase cocktails. *Eco* failed to grow on either xylan substrate and exhibited limited growth on oligosaccharides derived from them (Fig. 4*A* and *SI Appendix*, Fig. S13*A*), indicating it cannot directly access breakdown products from EM03. This points to a potential metabolic dependency on other community members for carbon acquisition. To identify such partners, we cocultured *Eco* with *Cbe*, *Cbu*, or *Cma* in biotin-deficient chemically defined media supplemented with xylan-derived oligosaccharides. Among the tested combinations, only the *Eco–Cbe* coculture promoted *Eco* growth (*SI Appendix*, Fig. S13*B*), indicating a possible cross-feeding interaction.

To further examine this interaction, we hydrolyzed beechwood xylan and wheat arabinoxylan using individually purified EM03-derived xylanases and used the resulting oligosaccharides as carbon sources in *Eco–Cbe* cocultures. *Eco* growth was supported only when cocultured with *Cbe* on oligosaccharides generated by GH11 xylanase 1087 (from beechwood xylan) or GH10 xylanase 1130 (from wheat arabinoxylan) (Fig. 4 *B* and *C* and *SI Appendix*, Fig. S13*C*). These results indicate that only the oligosaccharides produced by specific EM03-derived enzymes are further utilized by *Cbe*, leading to the production of monosaccharides that may become accessible to *Eco*. To confirm this, we analyzed xylose dynamics. Xylose accumulated in the supernatant of *Cbe* monocultures grown on 1130-derived oligosaccharides but was depleted in *Eco–Cbe* cocultures. Inhibiting *Eco* growth with polymyxin B led to increased xylose levels (Fig. 4*D*), confirming that *Eco* consumed xylose released from *Cbe*. Supplementing biotin-deficient media with xylose enhanced *Eco* growth (Fig. 4*E*), further supporting this conclusion. However, this raised the question of how the release of xylose is modulated in coculture with *Cbe*.

Since xylose production is linked to β-xylosidase activity, we measured β-xylosidase activity in *Cbe* monocultures and *Eco-Cbe* cocultures. Although overall β-xylosidase activity was higher in cocultures (*SI Appendix*, Fig. S13*D*), the per-cell enzyme activity was higher in *Cbe* monocultures (Fig. 4*F*), indicating lower per-cell enzyme secretion levels in coculture conditions. To explore the regulatory basis of this variation, we examined the genetic context of β-xylosidase genes (IDs: 2177 and 2178) in *Cbe* and identified an upstream xylose repressor gene, xylR (Fig. 4*G*). When xylose is present, XylR dissociates from the promoter region, allowing transcription of β-xylosidase genes (27). Structural predictions using Alphafold3 supported the binding of XylR to the target promoter (*SI Appendix*, Fig. S13*E*). Moreover, we observed that β-xylosidase secretion decreased as extracellular xylose levels declined in biotin-containing defined media (Fig. 4*G*), consistent with glycosidase secretion being regulated in response to extracellular xylose availability. This response likely minimizes unnecessary enzyme production under resource-limited conditions, which is associated with limited monosaccharide availability to rapidly growing nondegraders.

Together, these findings demonstrate that exploitation within EMSD5 is constrained by two interlinked processes. First, resource partitioning results from the substrate specificity of EM03-derived enzymes, which produce a diverse array of oligosaccharides, among which only those generated by specific enzymes become accessible to *Cbe*. Second, the level of glycosidase secretion in Cbe correlates with local xylose concentrations, with lower extracellular xylose associated with reduced enzyme secretion, thereby limiting further xylose release.

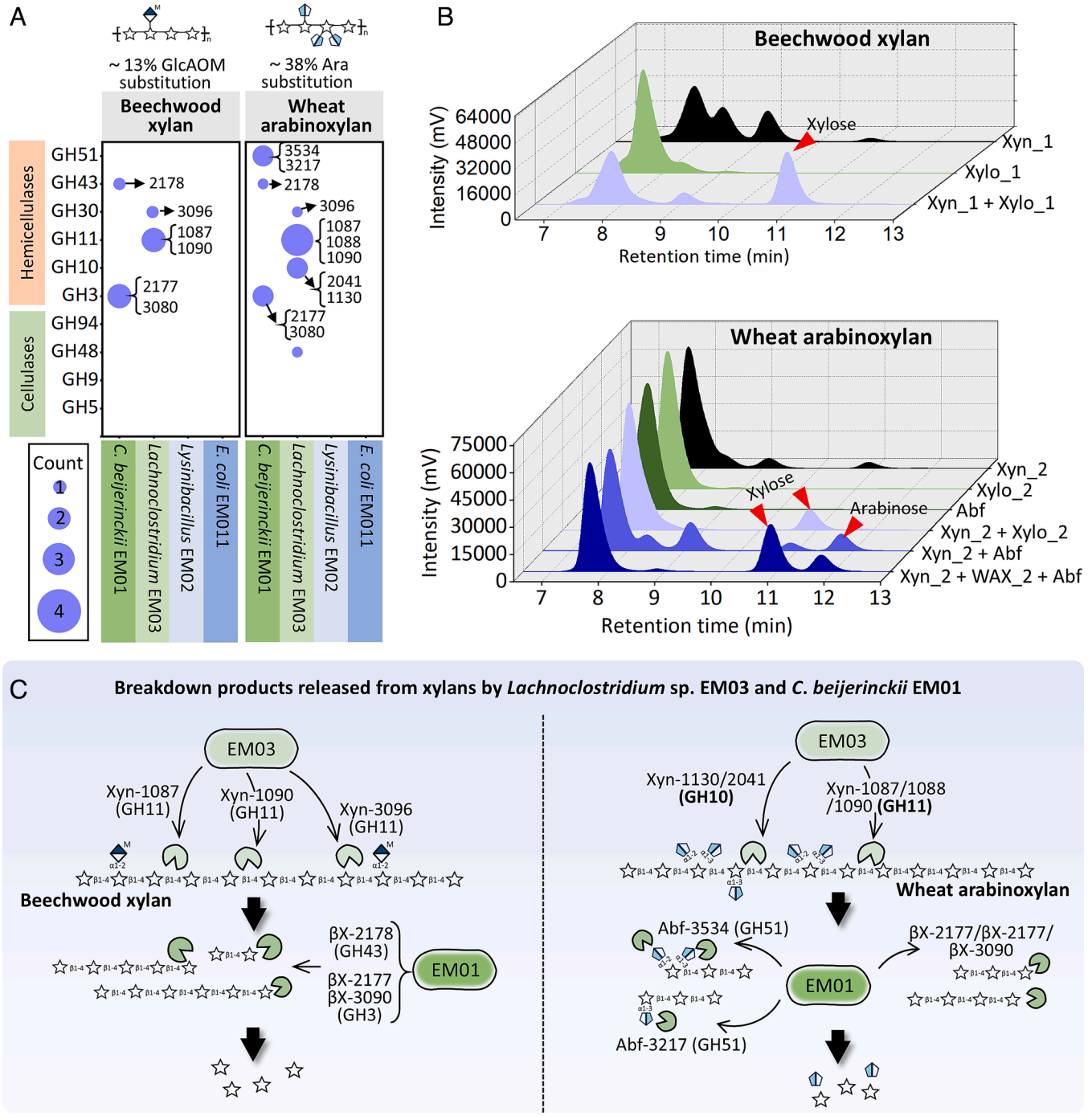

Fig. 3. Mutualistic interaction between *Lachnoclostridium* EM03 and *Clostridium beijerinckii* EM01 in the degradation of xylans. (*A*) LC–MS/MS analysis of hydrolase in the supernatant of EMSD5 under the induction of beechwood xylan and wheat arabinoxylan, respectively. All experiments were performed in triplicate, and enzymes present in all three replicates were counted. Detailed information can be found in *SI Appendix*, Fig. S8 and Dataset S4. (*B*) HPLC analysis of the breakdown products resulting from the treatment of beechwood xylan and wheat arabinoxylan with enzyme cocktails from EM03 and EM01, respectively. The enzyme composition of each cocktail and the reducing sugars produced by the enzyme cocktails, both separately and in combination, are detailed in *SI Appendix*, Figs. S11 and S12. (*C*) Schematic representation illustrating the mutualistic interactions of *Lachnoclostridium* sp. EM03 and *C. beijerinckii* EM01 in degrading beechwood xylan (*Left*) and wheat arabinoxylan (*Right*).

Beneficial Roles of *Escherichia* toward *Clostridium* are Widespread Across Lignocellulolytic Environments. We extended our investigation to explore the prevalence of the mutualistic relationship between *Escherichia* and *Clostridium* across various ecosystems. Surveying 337 microbial communities, we found that *Escherichia* and *Clostridium* coexisted at varying frequencies across different lignocellulolytic ecosystems: 95.6% in cow feces, 87.1% in pig feces, 55.0% in chicken feces, 33.3% in yak feces, and 25.2% in bovine rumen (Fig. 5*A*).

Phylogenetic analysis indicated that *E. coli* strains from fecal and ruminal habitats form distinct branches (Fig. 5*B*), reflecting possible divergence associated with host environment and microbial context. To assess the functional outcomes of this divergence, we tested the ability of various *E. coli* strains to enhance the growth of *Cbe* in the biotin-deficient chemically defined media (with 2 g/L xylose), including two strains from nonfecal sources—*E. coli* MG1655 and *E. coli* BW25113, as well as three strains from fecal sources—*E. coli* GZC 08-10, *E. coli* GZC 09-6, and *E. coli* LN67, along with *Eco* from

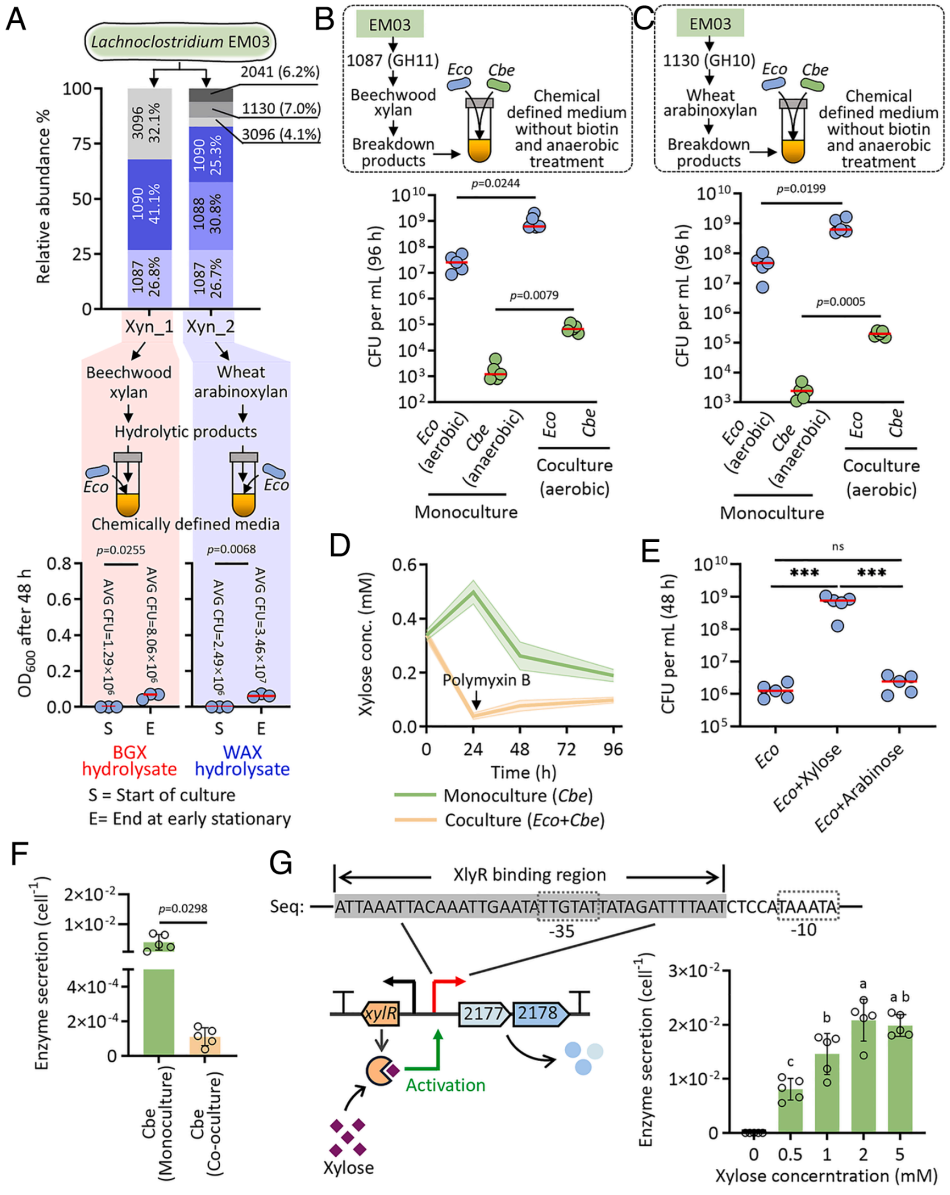

Fig. 4. Resource partitioning and enzyme feedback regulation in degraders constrain the availability of breakdown products to nondegraders. (*A*) Enzyme composition of the xylanase cocktail Xyn_1 and Xyn_2 derived from *Lachnoclostridium* sp. EM03. OD_{600} and CFU counts for *Eco* in biotin-deficient chemically defined media with the hydrolysates of beechwood xylan or wheat arabinoxylan generated by the corresponding xylanase cocktails from EM03 (n = 3). P values derived from paired two-tailed Student's t test. (*B*) Comparison of the number of CFU for *Eco* and *Cbe* as monocultures and as a coculture in the biotin-deficient chemically defined media with the hydrolysates of beechwood xylan treated by purified xylanase 1087 (GH11) as the carbon source. Mann–Whitney test for *Cbe* monoculture vs. *Cbe* coculture; Welch's t test for *Eco* monoculture vs. *Eco* coculture. (*C*) Comparison of the number of CFU for *Eco* and *Cbe* as monocultures and as a coculture in the biotin-deficient chemically defined media with the hydrolysates of wheat arabinoxylan treated by purified xylanase 1130 (GH10) as the carbon source, respectively (n = 5). P values derived from Welch's t test. (*D*) HPLC analysis of the concentrations of xylose in the supernatant of *Cbe* monoculture and in the coculture with *Eco* treated by polymyxin B at 24 h. (*E*) Growth of *Eco* in biotin-deficient chemically defined media supplemented with 5 mM of free sugars (n = 5). P values derived from one-way ANOVA with the Tukey test, statistical significance indicated as ***P < 0.001, "ns" for nonsignificant comparison. (*F*) Comparison of the secretion of β-xylosidase per cell for *Cbe* in monoculture and in coculture. Per cell enzyme secretion was calculated by dividing β-xylosidase activities (*SI Appendix*, Fig. S13*D*) in the supernatant by cell numbers determined through plating (Fig. 4*C*). Data are represented as mean ± SEM. P values derived from unpaired two-tailed Student's t test. (*G*) Schematic representation illustrating the detachment of the xylose repressor (XylR) from DNA upon binding to xylose, which allows transcription of genes 2177 and 2178. Secretion of β-xylosidase by *Cbe* with varying xylose concentrations in LB medium (n = 5), with enzyme secretion calculated by dividing β-xylosidase activities in the supernatant by cell growth. P values derived from one-way ANOVA with the Tukey test, with different letters indicating statistically significant differences.

EMSD5. We found that MG1655 and BW25113 failed to enhance the growth of *Cbe*. In contrast, the fecal-derived strains GZC 08-10, GZC 09-6, LN67, and *Eco* significantly promoted the growth of *Cbe* (Fig. 5*C*). Among these, *Eco* exhibited the highest efficiency, requiring the lowest *Eco*-to-*Cbe* CFU ratio to stimulate a unit increase in *Cbe* biomass (Fig. 5*D*). These results indicate that some fecal-derived *E. coli* strains can enhance *Clostridium* growth, likely through biotin or related metabolite cross-feeding, with variable facilitation efficiency among strains.

To explore the genetic basis of this facilitation, we analyzed the presence of biotin biosynthesis genes in *E. coli* and *Clostridium* genomes. *E. coli* strains universally possessed all the genes necessary for biotin synthesis, while *Clostridium* strains exhibited widespread deficiencies, particularly in *bioC, fabI, bioH, and bioF*. Expanding this analysis to 81 *Enterobacteriaceae* and 44 *Clostridiaceae* genomes revealed that 97.5% of *Enterobacteriaceae* strains possess a complete biotin biosynthesis pathway, while *Clostridiaceae* showed widespread gene loss consistent with the pattern in *Clostridium* (Fig. 5*E* and

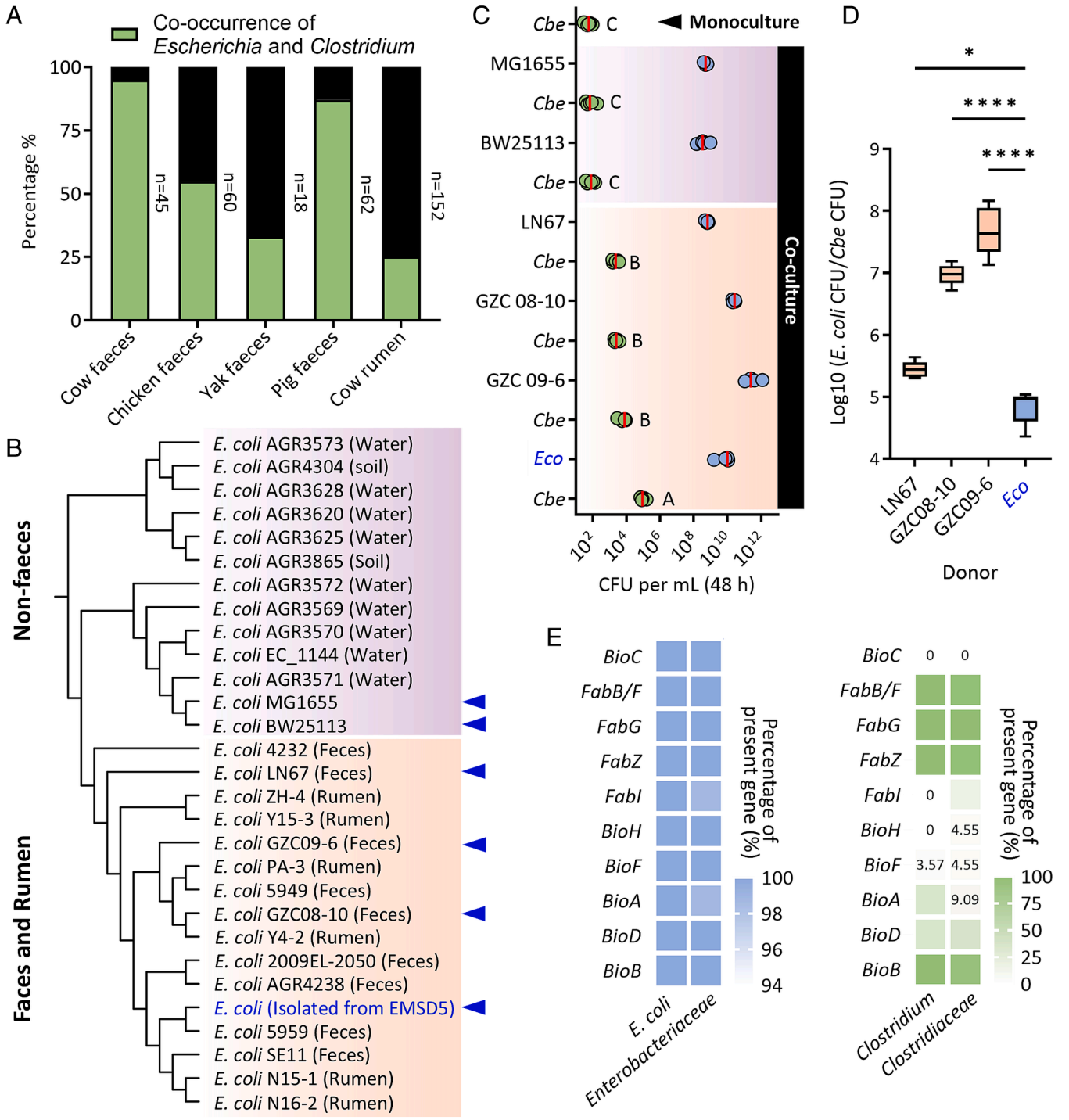

Fig. 5. *E. coli* within EMSD5 evolves in benefiting *Clostridium*. (*A*) Coexistence of *Escherichia* and *Clostridium* in different ecosystems, with the number of samples analyzed across these ecosystems shown. (*B*) Phylogenetic tree of *E. coli* strains isolated from various environmental samples. (*C*) The growth-promoting effect of *E. coli* from different sources on *C. beijerinckii* in biotin-deficient chemically defined media (n = 5). *P* values were derived from Welch's ANOVA with Dunnett's test, with different letters indicating significant differences. (*D*) Ratio of *E. coli* CFUs to *Cbe* CFUs within the coculture system. *P* values derived from Welch's ANOVA with Dunnett's test, statistical significance indicated as $*P < 0.05$, $****P < 0.0001$. (*E*) Percentage of genes involved in biotin synthesis pathways present in the genomes of 27 *E. coli* strains, 81 strains from the *Enterobacteriaceae* family, 28 *Clostridium* strains, and 44 strains from the *Clostridiaceae* family. The presence of individual biotin synthesis pathway genes in these genomes is detailed in Dataset S6.

Dataset S6). These findings suggest the potential for common biotin cross-feeding between *Escherichia* and *Clostridium* in lignocellulolytic environments.

Harnessing the Mutualism Between *Clostridium* and *Escherichia* Toward Hemicellulose Bioconversion. Building on the observed mutualistic interactions between degraders and between degraders and nondegraders, we engineered two synthetic microbial consortia to produce isopropanol from hemicellulose substrates, specifically beechwood xylan and wheat arabinoxylan. Due to challenges in isolating *Lachnoclostridium sp.* EM03, we heterologously expressed two essential cross-feeding xylanase genes, *xyn-1087* (GH11) and *xyn-1130* (GH10), in *Eco*, generating strains Eco-pETTac-1087 and Eco-pETTac-1130, respectively (Fig. 6*A*). Coculture of these engineered *E. coli* strains with *Cbe* enabled the degradation of xylans via functional complementarity. Additionally, *Eco* provided

anaerobic conditions that supported *Clostridium* growth, resulting in a streamlined consortium for hemicellulose bioconversion.

Functional evaluation of these consortia revealed that the Eco-pETTac-1087/*Cbe* combination produced 2.62 g/L isopropanol from beechwood xylan after 96 h, while the Eco-pETTac-1130/*Cbe* consortium achieved higher production (3.21 g/L) from wheat arabinoxylan (Fig. 6 *B* and *C*). This enhanced production with wheat arabinoxylan likely stems from its breakdown products, which, when treated with xylanase 1130, stimulated higher activities of α-L-arabinofuranosidase and β-xylosidase in *Cbe* compared to beechwood xylan treated with xylanase 1087 (*SI Appendix*, Fig. S14). Additionally, by efficiently consuming accumulated oligosaccharides, *Cbe* alleviated potential feedback inhibition on xylanase activity (Fig. 6 *B* and *C*).

Inoculation ratio optimization revealed that increasing the *Eco*:*Cbe* ratio to 5:1 significantly enhanced early-stage (12 h) isopropanol production compared to the 1:1 control for both substrates. However, this early advantage diminished by 24 h and did not affect the final isopropanol titer. Reducing the *Eco* inoculum (1:2 or 1:5) only led to insignificant decreases in early production (*SI Appendix*, Fig. S15). These results suggest that the final production performance is inoculation ratio-independent, highlighting the robustness of the *Eco*–*Cbe* mutualism.

To evaluate the system's versatility, we extended our investigation by substituting *C. beijerinckii* with another solvent-producing *Clostridium*, *C. acetobutylicum* CICC8016, to produce acetone–butanol–ethanol. The engineered consortium successfully converted beechwood xylan into 0.49 g/L acetone, 1.19 g/L butanol, and 0.13 g/L ethanol, and wheat arabinoxylan into 0.30 g/L acetone and 0.65 g/L butanol (Fig. 6 *D* and *E*).

These findings highlight the critical role of *Cbe-Eco* mutualism in lignocellulose-to-isopropanol conversion while demonstrating the generalizability of this framework to other solventogenic clostridia, supporting its broad applicability for biomass conversion.

Discussion

Microbiomes drive the global biogeochemical cycles (28), with their composition and dynamics heavily influenced by nutrient availability (29, 30). Recent analyses of diverse environments have shown that microbiota dominated by cooperation are more resilient to nutrient fluctuations (31). This finding indicates that interspecies interactions also influence community assembly. While several studies have employed synthetic consortia to investigate how interactions shape niches of community members (32, 33), we still lack empirical evidence from natural ecosystems.

Due to the inherent complexity of natural microbiomes, direct investigation into these communities is often challenging (34). To address this, we enriched a lignocellulose-degrading consortium, EMSD5, from compost. By using frozen stock cultures as a consistent inoculum source and employing standardized resuscitation protocols, EMSD5 maintains a reproducible community structure across successive transfers (21, 22, 35). Within this stable consortium, we observed direct evidence of niche expansion between both distantly and closely related species.

Among distantly related species, *E. coli* facilitates the survival of *Clostridium* in initially aerobic environments (Fig. 2), while *Clostridium* enables *Eco* to thrive on polysaccharides. Unlike previous studies of pollutant- or lignin-degrading communities, where nondegraders provide essential metabolites (19, 36–39), we show that nondegraders expand the ecological niche of degraders by providing anoxic conditions and biotin, allowing survival in otherwise inhospitable environments. The enhanced mutualistic capacity of habitat-derived *Eco* strains (Fig. 5*C*) likely stems from multiple adaptations: superior anaerobic growth enabling early biotin provision, optimized biotin production and secretion, or potentially other metabolite exchange. While metabolite exchange is widespread among microbes (40), the *Eco-Cbe* interaction described here appears to be genuinely cooperative, as both partners invest substantially in metabolite production, with costs supported by established literature (41–43). Additionally, this reciprocal exchange may be refined by adaptations in *Eco* that increase benefits to *Clostridium* (Fig. 5*D*). Such cooperative relationships between distantly related species are rarely documented. The difficulty in isolating EM03, a species with average nucleotide identity values below 81% relative to known genomes (*SI Appendix*, Fig. S16 and Table S3), may be due to its obligate dependence on cooperative interactions within EMSD5.

Among closely related species, *Lachnoclostridium sp.* expands the niche of *Cbe* by hydrolyzing polysaccharides into oligosaccharides (Fig. 4). Although the mutualistic interaction mediated by functionally complementary enzymes is widespread in nature (7, 44), few studies have explored how these enzymes work together to achieve this mutualistic interaction, and the ecological implications of such cooperation remain unclear. Our data reveal how enzyme-mediated interactions between closely related species enhance mutualism and ecological niche breadth. This dynamic may also occur in other systems, such as chitin-degrading ecosystems, where phylogenetically related strains often coexpress complementary enzymes (2, 5). Future research should explore how phylogenetic distance influences the extent of niche expansion, particularly in extracellular enzyme-driven systems.

A key question in biological cooperation is how polymer-degrading cells avoid being outcompeted by nonproducing exploiters (1, 13). Some microbes mitigate this by anchoring enzymes to the cell surface (45), or by secreting oligomers that are selectively accessible (46). In EMSD5, a more sophisticated scenario is observed: Xylanases with distinct substrate specificities produced by EM03 lead to the formation of both inaccessible and cross-feeding oligosaccharides (Fig. 4 *A*–*C*). A subset of these oligosaccharides is utilized by *Cbe*, which is associated with glycosidase secretion, generating monosaccharides that support the transient growth of *Eco* (Fig. 4 *D* and *E*). Moreover, glycosidase secretion in *Cbe* decreased as extracellular xylose levels declined, thereby reducing the availability of monosaccharides to *Eco* (Fig. 4*F*). These findings highlight interlinked interactions among degraders that constrain exploitation.

In biofuel production, polysaccharide-degrading microbes are typically cocultured with solvent producers, yet these artificial consortia often face fundamental ecological challenges including niche separation (47) and carbon competition (48). By leveraging niche-expanding interactions and regulatory strategies found in EMSD5, we engineered *E. coli* to express a cross-feeding xylanase gene derived from EM03. This engineered system successfully established a cooperative niche and controlled carbon flow to *C. beijerinckii* while minimizing competitive interactions from *E. coli* (Fig. 6 *B* and *C*). Although this framework was extended to *C. acetobutylicum* CICC8016, its solvent yield was lower than in the isopropanol-producing system. This discrepancy is likely due to CICC8016's inability to efficiently utilize the hydrolysates released by the cross-feeding xylanase, underscoring the finely tuned mutualism among the native degraders within EMSD5. Although the synthetic consortium produced less isopropanol than the native EMSD5, it underscores the essential role of these interactions in lignocellulose conversion. A complete understanding of EMSD5, including the roles of *Bacteroides*, could further inform the design of high-performing synthetic consortia.

In conclusion, our study reveals the mutualism between degraders and nondegraders that stabilizes the structure and function of lignocellulose-converting communities. Nondegraders pioneer niche creation, enabling degrader activity. Meanwhile, distinct

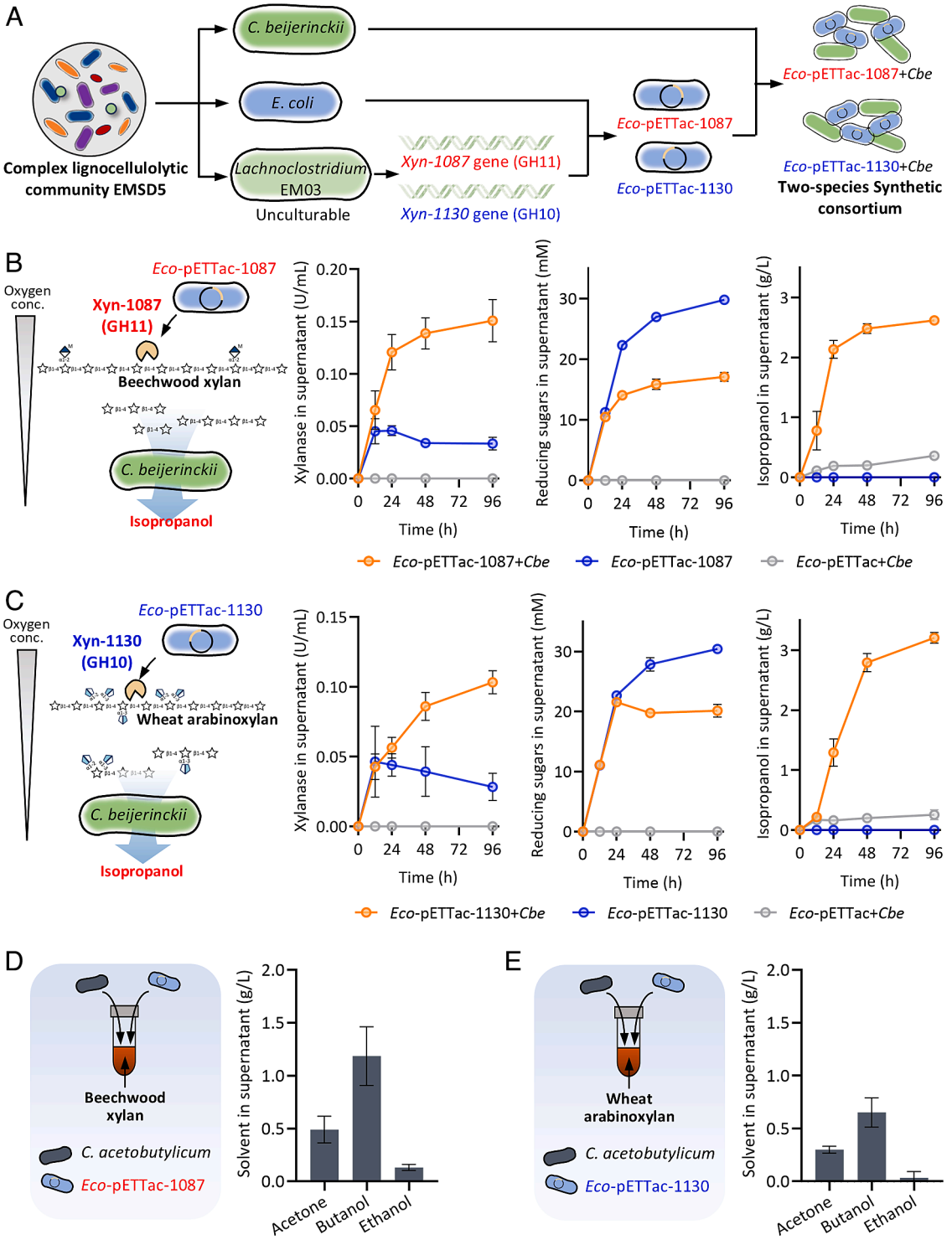

Fig. 6. Isopropanol and acetone–butanol–ethanol production from xylans by synthetic consortium constructed using *Clostridium* and an engineered *E. coli*. (*A*) Schematic for the engineering of *E. coli* (*Eco*-pETTac-1087 and *Eco*-pETTac-1130) and for construction of a synthetic consortium. (*B*) HPLC analysis of isopropanol production from beechwood xylan by the synthetic consortium consisting of *Eco*-pETTac-1087 and *Cbe*, alongside measurements of xylanase activity and reducing sugars (n = 3). (*C*) HPLC analysis of isopropanol production from wheat arabinoxylan by the synthetic consortium consisting of *Eco*-pETTac-1130 and *Cbe*, with corresponding measurements of xylanase activity and reducing sugars (n = 3). (*D*) HPLC analysis of acetone–butanol–ethanol production after 96-h fermentation from beechwood xylan by synthetic consortium consisting of *Eco*-pETTac-1087 and *C. acetobutylicum* CICC8016 (n = 3). (*E*) HPLC analysis of acetone–butanol–ethanol production after 96-h fermentation from wheat arabinoxylan by synthetic consortium consisting of *Eco*-pETTac-1130 and *C. acetobutylicum* CICC8016 (n = 3). Data are presented as mean ± SEM.

mechanisms observed in different degraders constrain the accessibility of breakdown products to nondegraders, thereby maintaining the structural and functional stability of the community. These findings highlight the ecological significance of these interactions and provide strategies for balancing these interactions in biopolymer-converting consortia.

Materials and Methods

Seed Culture Preparation and Isopropanol Production From Corncob by EMSD5. Five *E. coli* strains, including *E. coli* 1655, *E.* coli BW25113, *E. coli* LN67, *E. coli* GZC09-6, and *E. coli* GZC08-10, used in this study were preserved in 25% glycerol (v/v) at −70 °C and grown in LB medium at 37 °C with shaking (200 rpm) prior to experiments.

EMSD5 seed cultures were preserved similarly. Before corncob conversion, the seed culture was cultivated in PCS medium (21) statistically at 37 °C with three consecutive passages (8%, v/v, of inoculum). Corncob bioconversion was carried out at 32 °C in a 100-mL Erlenmeyer flask containing 65 mL of medium optimized in a prior study (22), comprising (per liter): Yeast Extract, 5 g; Tryptone, 10 g; NaCl, 5 g; corncob, 40 g; adjusted to pH 7.0. Samples were taken on days 1, 2, 4, and 6, corresponding to the initial, rapid, and stagnation phases of isopropanol production, respectively, as defined in the previous study (22).

Community Structure and Function Analysis. To investigate the bacterial community dynamics, microbial genomic DNA was extracted from EMSD5 samples using a TIANamp DNA Extraction Kit (TIAN-GEN, Beijing, China). PCR amplification targeted the V3-V4 regions of the 16S rRNA gene, and amplicons were sequenced on the Illumina Hiseq platform (Novogene, Beijing, China). Raw DNA sequences are deposited under BioProject PRJNA918848 (*SI Appendix*, Table S4) on the NCBI website. Detailed methods for raw sequence processing and community structure analysis are provided in the *SI Appendix*.

To explore functional roles, genomic DNA from EMSD5 cultures incubated with corncob for 6 d was assessed using agarose gel electrophoresis and a Nanophotometer P300 (IMPLEN, Germany). High-quality DNA was sequenced on the Illumina HiSeq 2500 PE150 platform (Magigene, Guangzhou, China), with sequences available under BioProject PRJNA918781 on the NCBI website. Methods for raw read processing, assembly, genome binning, taxonomic classification, and pathway analysis, are detailed in the *SI Appendix*.

Isolation, Molecular Identification and Functional Characterization of Strains from EMSD5. To isolate aerobes/facultative anaerobes, 100 μL of diluted EMSD5 culture (10^{-5}) was streaked onto LB plates and incubated aerobically at 37 °C for 48 h, then the occurred colonies were purified through repeated streaking. For *Clostridium* strains, isolation was conducted using NBRC medium (49) with 5 g/L cellobiose. After 6 days of culture, diluted EMSD5 (10^{-5}) was streaked onto solid plates and incubated anaerobically for 4 days. All procedures for *Clostridium* strains were performed in an anaerobic glove box. Genomic DNA was extracted using the TIANamp DNA Extraction Kit, and the 16S rRNA gene was amplified with primers 27F and 1492R. PCR products were sequenced in Beijing Genomics Institute and the acquired sequences were aligned using NCBI BLAST.

C. beijerinckii (*Cbe*) cultures were grown in NBRC medium with 5 g/L cellobiose (OD600 ~1.0) and inoculated (2%) into serum bottles containing 50 mL NBRC medium with glucose, xylose, cellobiose, or xylobiose (50 g/L). Samples were collected at 36 h, and isopropanol was quantified via HPLC (parameters in *SI Appendix*).

In Vitro Assessment of Vitamin Auxotrophies. Auxotrophies for riboflavin (B2), biotin (B7), and folate (B9) were evaluated by omitting each vitamin from chemically defined medium (composition in *SI Appendix*, Table S5). Controls included complete and vitamin-free chemically defined media. To minimize nutrient carryover, inocula were sequentially passaged three times in vitamin-free chemically defined media before use. Cultures were inoculated at $OD_{600} = 0.1$ into Hungate tubes with 10 mL chemically defined media under a nitrogen atmosphere. Tubes were incubated statically at 37 °C, and growth was monitored at OD600.

Coculture Experiments. To test the role of *E. coli* in creating anoxic conditions for *Clostridium*, equal volumes of *E. coli* and *C. beijerinckii* (mid-log phase, OD600 = 0.1) were coinoculated (1% inoculation volume each) into nutrient-rich medium (LB + 2 g/L xylose). Monocultures of each strain served as controls. After 48 h, cultures were diluted and spread onto LB plates (with 2 g/L xylose) and incubated at 37 °C for colony-forming unit (CFU) counting. To test biotin cross-feeding between *E. coli* and *Clostridium*, equal amounts of each strain (OD600 = 0.1) were coinoculated (each 1% of inoculation) into biotin-free chemically defined media. Monocultures in the same medium served as controls. The inocula were preconditioned by three passages in biotin-free chemically defined media to minimize residual biotin carryover. At specific intervals, cultures were diluted and plated on LB for CFU enumeration. To selectively count *Clostridium*, polymyxin B (10 mg/L) was added to the LB plates to inhibit *E. coli*. All procedures for *Clostridium* were performed in a glove box.

Measurement of Biotin Concentration in Supernatant. The biotin concentration in supernatant was detected using the Biotin Quantitative Kit (Elabscience). Briefly, 50 μL sample was added in determine wells and then added 50 μL Avidin-HRP. After 30 min incubation at 37 °C, the solution in each well was decanted and each well was washed using wash buffer for 3 times. 90 μL Tetramethylbenzidine (TMB) was added in each well. After incubating at 37 °C for about 15 min, 50 μL stop solution was added in each well and measured at 450 nm. Biotin concentration in supernatant was calculated using the standard curve of biotin.

Genome Editing and Overexpression in *E. coli*. A two-plasmid CRISPR/Cas9 system was used, comprising the pEcCas (Addgene plasmid no. 73227) and pEcgRNA (Addgene plasmid no. 166581) plasmids (50). T Target-specific dsDNA was generated by annealing 24-nt single-stranded oligonucleotides (4-nt overhangs and 20-nt target sequences) and ligated into *Bsa*I-linearized pEcgRNA to produce a target-specific plasmid (details in *SI Appendix*).

The pEcCas plasmid was electroporated into *E. coli* using a 0.1 cm-gap cuvette at 1.8 kV. Kanamycin-resistant transformants (50 μg/mL) were used to select electrocompetent cells. The λ-Red system was induced by adding 10 mM arabinose. The pEcgRNA plasmid, containing the PAM-targeting site and donor DNA fragment (amplification primers listed in *SI Appendix*, Table S6), was cotransformed. Edited monoclonal colonies were screened on selective media, and plasmids pEcgRNA and pEcCas were sequentially cured with rhamnose and sucrose, respectively.

For overexpression, the *aasS* gene from *Vibrio harveyi* (24) (GenBank: DQ525851.1) was codon-optimized for *E. coli* (Sangon Biotech Co., Ltd) and synthesized with *Hind*III and *Bam*HI restriction sites. The gene was ligated into pTrc99a, predigested with *Hind*III and *Bam*HI, using T4 DNA ligase. Overexpression of *aasS* was induced with 0.1 mM IPTG.

Extracellular Metaproteome Analysis. To profile extracellular GHs responsible for corncob degradation, liquid chromatography–tandem mass spectrometry (LC–MS/MS) was used to analyze supernatants of EMSD5 cultures induced by untreated corncob, hemicellulose (beechwood xylan and wheat arabinoxylan), and cellulose (filter paper). Details of GH identification in the supernatants are provided in the *SI Appendix*.

Enzyme Cocktail Construction and Hydrolysis. Heterologous expression and hydrolysate analysis of GHs are described in the SI. Enzyme cocktails were prepared based on emPAI-derived abundances (Dataset S5), and the composition of each enzyme cocktail is provided in *SI Appendix*. Hydrolysis reactions were carried out in a 1 mL mixture containing 20 mM Tris-HCl (pH 6.0), 1% (w/v) substrate, and 200 nM enzyme cocktail. The mixture was incubated at 45 °C, and hydrolysis products were analyzed by HPLC. Reducing sugars were quantified using the DNS method described by Miller et al (51).

Preparation of Chemical-Defined Medium Containing Different Hydrolysates. Hydrolysates were prepared by mixing beechwood xylan or wheat arabinoxylan (1% w/v) with enzyme cocktails or individual xylanases. All reactions were carried out at a final enzyme concentration of 200 nM in 20 mM Tris-HCl buffer (pH 6.0) at 45 °C for 12 h, until reducing sugar concentration plateaued. Posthydrolysis, the compounds of chemically defined medium without xylose were added to each hydrolysate and sterilized via a 0.22 μm filter. The sterilized media were then used to culture *Cbe* and *Eco*.

Measurement of Activities of Enzymes in the Supernatant. The β-xylosidase activity was measured using *p*-nitrophenyl xylopyranoside (*p*NPX) as the substrate. A reaction mixture of 50 μL cell-free supernatant and 50 μL of 2 mM *p*NPX in PBS buffer (pH 6.0) was incubated at 45 °C for 10 min. The reaction was stopped by adding 50 μL of 1 M Na_2CO_3, and the absorbance at 405 nm was measured. Enzyme activity was calculated from a standard curve of *p*-nitrophenol, with one unit defined as the amount of enzyme releasing 1 μmol of *p*-nitrophenol per minute. Xylanase activity, using beechwood xylan as a substrate, and the concentration of reducing sugars in the supernatant (in Fig. 6) were determined via the DNS method.

Genomic Data Collection. To explore the co-occurrence of *Clostridium* and *Escherichia*, 16S rRNA sequencing data were retrieved from the Sequence Read Archive (SRA). Detailed raw data accession numbers and data processing workflows are provided in the *SI Appendix*. To investigate the prevalence of biotin cross-feeding between *Clostridium* and *Escherichia*, we collected 27 *E. coli* genomes, 81 genomes from *Enterobacteriaceae* family, 28 genomes from *Clostridium*, and 44 genomes from *Clostridiaceae* family from RefSeq database or Genbank. Gene annotation for all genome sequences was performed using the same workflow described in *SI Appendix*. A phylogenetic tree of *E. coli* was constructed based on multicopy orthologous genes, with further details on the tree-building methodology provided in *SI Appendix*.

Establishment of Synthetic Consortium. Genes 1087 and 1130 from EMSD5 were amplified, digested with *Sal*I and *Not*I, and ligated into the pET-Tac vector (a modified pET22b(+) with a Tac promoter). Recombinant plasmids were transformed into *E. coli* from EMSD5, creating Eco-pETTac-1087 and Eco-pETTac-1130 strains.

Equal amounts of mid-log phase engineered *E. coli* and *Clostridium* (adjusted to OD600 = 0.1) were coinoculated into medium containing 5 g/L Yeast Extract, 10 g/L Tryptone, 5 g/L NaCl, 2 g/L $CaCO_3$, and 20 g/L beechwood or wheat arabinoxylan. Ampicillin (5 mg/L) maintained plasmid stability in *E. coli*. After 3 h at 37 °C, IPTG (0.1 mM) was added to induce the expression of 1087 and 1130. Samples (200 μL) were collected at 12, 24, 48, and 96 h for analysis of solvent production, reducing sugars, and xylanase activities. Solvents were quantified using HPLC.

Statistical Analysis. GraphPad Prism 10 was used for data analysis and visualization. Statistical details, including significance tests, are provided in the figure captions.

Data, Materials, and Software Availability. Metagenomic data associated with this project can be found at the NCBI under BioProject PRJNA918781 (52). Illumina HiSeq metagenomic data can be found under BioSample SAMN32605734. The data of 16S rRNA gene amplicon sequence can be found under BioProject PRJNA918848 (53); the BioSample number of each sample can be found in *SI Appendix*, Table S5. All study data are included in the article and/or supporting information.

ACKNOWLEDGMENTS. We would like to thank Prof. Yang Wang and Dr. Lu Yang for generously providing *E. coli* LN67, *E. coli* GZC09-6, and *E. coli* GZC08-10. We also extend our gratitude to Dr. Glen D'Souza from Arizona State University for his valuable and critical discussions regarding this work. This work was supported by Grants from the National Key Research and Development Program (grant no. 2022YFA0912103) and the 2115 Talent Development Program of China Agricultural University.

Author affiliations: [a]Department of Microbiology and Immunology, State Key Laboratory of Animal Biotech Breeding, and Key Laboratory of Soil Microbiology, Ministry of Agriculture, College of Biological Sciences, China Agricultural University, Beijing 100193, China; [b]Department of Microbiology and Immunology, State Key Laboratory of Plant Environmental Resilience, and Key Laboratory of Soil Microbiology, Ministry of Agriculture, College of Biological Sciences, China Agricultural University, Beijing 100193, China; [c]Department of Environmental Systems Science, Swiss Federal Institute of Technology Zürich, Zürich 8092, Switzerland; [d]Department of Environmental Microbiology, Eawag, Dübendorf 8600, Switzerland; and [e]Departamento de Microbiología, Escuela Nacional de Ciencias Biológicas, Instituto Politécnico Nacional, Mexico City 11340, Mexico

Author contributions: J.Y. and H.Y. designed research; L.L., Y.H., T.J., H.Z., and Q.Y. performed research; L.L., C.T., M.W., and Y.L. analyzed data; and L.L. and E.W. wrote the paper.

1. D. J. Jiménez *et al.*, Ecological insights into the dynamics of plant biomass-degrading microbial consortia. *Trends Microbiol.* **25**, 788–796 (2017).
2. S. Pontrelli *et al.*, Metabolic cross-feeding structures the assembly of polysaccharide degrading communities. *Sci. Adv.* **8**, eabk3076 (2022).
3. F. Azam, F. Malfatti, Microbial structuring of marine ecosystems. *Nat. Rev. Microbiol.* **5**, 782–791 (2007).
4. I. Vanwonterghem, P. D. Jensen, K. Rabaey, G. W. Tyson, Genome-centric resolution of microbial diversity, metabolism and interactions in anaerobic digestion. *Environ. Microbiol.* **18**, 3144–3158 (2016).
5. I. Raimundo *et al.*, Functional metagenomics reveals differential chitin degradation and utilization features across free-living and host-associated marine microbiomes. *Microbiome* **9**, 43 (2021).
6. L. M. Solden *et al.*, Interspecies cross-feeding orchestrates carbon degradation in the rumen ecosystem. *Nat. Microbiol.* **3**, 1274–1284 (2018).
7. S. R. Lindemann, A piece of the pie: Engineering microbiomes by exploiting division of labor in complex polysaccharide consumption. *Curr. Opin. Chem. Eng.* **30**, 96–102 (2020).
8. T. N. Enke *et al.*, Modular assembly of polysaccharide-degrading marine microbial communities. *Curr. Biol.* **29**, 1528–1535.e1526 (2019).
9. J. Gore, H. Youk, A. van Oudenaarden, Snowdrift game dynamics and facultative cheating in yeast. *Nature* **459**, 253–256 (2009).
10. M. S. Datta, E. Sliwerska, J. Gore, M. F. Polz, O. X. Cordero, Microbial interactions lead to rapid micro-scale successions on model marine particles. *Nat. Commun.* **7**, 11965 (2016).
11. P. Smith, M. Schuster, Public goods and cheating in microbes. *Curr. Biol.* **29**, R442–R447 (2019).
12. S. Pollak *et al.*, Public good exploitation in natural bacterioplankton communities. *Sci. Adv.* **7**, eabi4717 (2021).
13. K. Drescher, Carey D. Nadell, Howard A. Stone, Ned S. Wingreen, Bonnie L. Bassler, Solutions to the public goods dilemma in bacterial biofilms. *Curr. Biol.* **24**, 50–55 (2014).
14. C. E. Lawson *et al.*, Metabolic network analysis reveals microbial community interactions in anammox granules. *Nat. Commun.* **8**, 15416 (2017).
15. S. Pande *et al.*, Privatization of cooperative benefits stabilizes mutualistic cross-feeding interactions in spatially structured environments. *ISME J.* **10**, 1413–1423 (2016).
16. D. Preussger, S. Giri, L. K. Muhsal, L. Oña, C. Kost, Reciprocal fitness feedbacks promote the evolution of mutualistic cooperation. *Curr. Biol.* **30**, 3580–3590.e3587 (2020).
17. S. Giri, S. Waschina, C. Kaleta, C. Kost, Defining division of labor in microbial communities. *J. Mol. Biol.* **431**, 4712–4731 (2019).
18. G. D'Souza *et al.*, Interspecies interactions determine growth dynamics of biopolymer-degrading populations in microbial communities. *Proc. Natl. Acad. Sci. U.S.A.* **120**, e2305198120. (2023).
19. Q. Peng *et al.*, Modeling bacterial interactions uncovers the importance of outliers in the coastal lignin-degrading consortium. *Nat. Commun.* **16**, 639 (2025).
20. S. Paul, A. Dutta, Challenges and opportunities of lignocellulosic biomass for anaerobic digestion. *Resour. Conserv. Recycl.* **130**, 164–174 (2018).
21. Z. Lv, J. Yang, H. Yuan, Production, purification and characterization of an alkaliphilic endo-β-1, 4-xylanase from a microbial community EMSD5. *Enzyme Microb. Technol.* **43**, 343–348 (2008).
22. L. Liu *et al.*, Consolidated bioprocessing performance of bacterial consortium EMSD5 on hemicellulose for isopropanol production. *Bioresour. Technol.* **292**, 121965 (2019).
23. M. Z. DeMaere, A. E. Darling, Bin3C: Exploiting Hi-C sequencing data to accurately resolve metagenome-assembled genomes. *Genome Biol.* **20**, 46 (2019).
24. Y. Jiang, C. H. Chan, J. E. Cronan, The soluble acyl-acyl carrier protein synthetase of *Vibrio harveyi* B392 is a member of the medium chain acyl-CoA synthetase family. *Biochemistry* **45**, 10008–10019 (2006).
25. M. Gralka, R. Szabo, R. Stocker, O. X. Cordero, Trophic interactions and the drivers of microbial community assembly. *Curr. Biol.* **30**, R1176–R1188 (2020).
26. P. J. Smith, H.-T. Wang, W. S. York, M. J. Peña, B. R. Urbanowicz, Designer biomass for next-generation biorefineries: Leveraging recent insights into xylan structure and biosynthesis. *Biotechnol. Biofuels* **10**, 286 (2017).
27. K. Zhang *et al.*, Genome-scale metabolic model of *Caldicellulosiruptor bescii* reveals optimal metabolic engineering strategies for bio-based chemical production. *mSystems* **6**, e0135120 (2021), 10.1128/msystems.01351-01320.
28. N. W. Sokol *et al.*, Life and death in the soil microbiome: How ecological processes influence biogeochemistry. *Nat. Rev. Microbiol.* **20**, 415–430 (2022).
29. M. Dal Bello, H. Lee, A. Goyal, J. Gore, Resource–diversity relationships in bacterial communities reflect the network structure of microbial metabolism. *Nat. Ecol. Evol.* **5**, 1424–1434 (2021).
30. Y. Miao *et al.*, A novel decomposer-exploiter interaction framework of plant residue microbial decomposition. *Genome Biol.* **26**, 20 (2025).
31. D. Machado *et al.*, Polarization of microbial communities between competitive and cooperative metabolism. *Nat. Ecol. Evol.* **5**, 195–203 (2021).
32. L. Oña *et al.*, Obligate cross-feeding expands the metabolic niche of bacteria. *Nat. Ecol. Evol.* **5**, 1224–1232 (2021).
33. J. Russel, H. L. Røder, J. S. Madsen, M. Burmølle, S. J. Sørensen, Antagonism correlates with metabolic similarity in diverse bacteria. *Proc. Natl. Acad. Sci. U.S.A.* **114**, 10684–10688 (2017).
34. X. N. Peng, S. P. Gilmore, M. A. O'Malley, Microbial communities for bioprocessing: Lessons learned from nature. *Curr. Opin. Chem. Eng.* **14**, 103–109 (2016).
35. N. Zhu *et al.*, Metagenomic and metaproteomic analyses of a corn stover-adapted microbial consortium EMSD5 reveal its taxonomic and enzymatic basis for degrading lignocellulose. *Biotechnol. Biofuels* **9**, 243 (2016).
36. X. Xu *et al.*, Modeling microbial communities from atrazine contaminated soils promotes the development of biostimulation solutions. *ISME J.* **13**, 494–508 (2019).
37. K. Yu *et al.*, An integrated meta-omics approach reveals substrates involved in synergistic interactions in a bisphenol A (BPA)-degrading microbial community. *Microbiome* **7**, 16 (2019).
38. B. Hu *et al.*, Metabolic exchange with non-alkane-consuming *Pseudomonas stutzeri* SLG510A3-8 improves n-alkane biodegradation by the alkane degrader *Dietzia* sp. strain DQ12-45-1b. *Appl. Environ. Microbiol.* **86**, e02931-19 (2020).
39. X. Wang *et al.*, Nitrogen transfer and cross-feeding between *Azotobacter chroococcum* and *Paracoccus aminovorans* promotes pyrene degradation. *ISME J.* **17**, 2169–2181 (2023).
40. G. D'Souza *et al.*, Ecology and evolution of metabolic cross-feeding interactions in bacteria. *Nat. Prod. Rep.* **35**, 455–488 (2018).
41. S. Rakoff-Nahoum, K. R. Foster, L. E. Comstock, The evolution of cooperation within the gut microbiota. *Nature* **533**, 255–259 (2016).
42. G. D'Souza, C. Kost, Experimental evolution of metabolic dependency in bacteria. *PLoS Genet.* **12**, e1006364 (2016).
43. G. D'Souza *et al.*, Less is more: Selective advantages can explain the prevalent loss of biosynthetic genes in bacteria. *Evolution* **68**, 2559–2570 (2014).
44. H. Zheng *et al.*, Division of labor in honey bee gut microbiota for plant polysaccharide digestion. *Proc. Natl. Acad. Sci. U.S.A.* **116**, 25909 (2019).
45. L. Artzi, E. A. Bayer, S. Moraïs, Cellulosomes: Bacterial nanomachines for dismantling plant polysaccharides. *Nat. Rev. Microbiol.* **15**, 83–95 (2017).
46. F. Cuskin *et al.*, Human gut *Bacteroidetes* can utilize yeast mannan through a selfish mechanism. *Nature* **517**, 165–169 (2015).
47. S. Ben Said, R. Tecon, B. Borer, D. Or, The engineering of spatially linked microbial consortia – Potential and perspectives. *Curr. Opin. Biotechnol.* **62**, 137–145 (2020).
48. Y. Jiang *et al.*, Recent advances of biofuels and biochemicals production from sustainable resources using co-cultivation systems. *Biotechnol. Biofuels* **12**, 155 (2019).
49. B. Mohtasebi, M. Maki, W. Qin, Y. Dahman, Novel fusants of two and three clostridia for enhanced green production of biobutanol. *Biofuels* **12**, 1–11 (2019).
50. Q. Li *et al.*, A modified pCas/pTargetF system for CRISPR-Cas9-assisted genome editing in Escherichia coli. *Acta Biochim. Biophys. Sin.* **53**, 620–627 (2021).
51. G. L. Miller, Use of dinitrosalicylic acid reagent for determination of reducing sugar. *Anal. Chem.* **31**, 426–428 (1959).
52. L. Liu, "Metagenomic data obtained from decomposition *microbiome* EMSD5 enriched from compost soil." NCBI Sequence Read Archive, PRJNA918781. https://www.ncbi.nlm.nih.gov/bioproject/?term=PRJNA918781. Accessed 5 January 2023.
53. L. Liu, "Analysis of the structure of decomposition microbiota enriched from compost soil." NCBI Sequence Read Archive, PRJNA918848. https://www.ncbi.nlm.nih.gov/bioproject/?term=PRJNA918848. Accessed 6 January 2023.